JOURNAL OF GEOPHYSICAL RESEARCH, VOL. 103, NO. C11, PAGES 24,675-24,691, OCTOBER 15, 1998

Ice thickness variability, isostatic balance and potential for snow ice formation on ice floes in the south polar Pacific Ocean

Ute Adolphs[1]

Geophysical Institute, University of Alaska, Fairbanks

Abstract. Spatial and temporal characteristics of snow and ice thickness were determined for data, acquired during five cruises into the Bellingshausen/Amundsen and Ross Seas between September 1993 and 1995. When sorted into distance classes from the ice edge, snow and ice thicknesses show a pattern of spatial and temporal variability that reflects the relative regional importance of different sea ice growth mechanisms, motion and deformation as well as of oceanographic processes. The potential for snow ice formation was directly investigated for the drilling data. Flooding, measured prior to drilling, has a strong correspondence with negative freeboard, while moist snow shows a lesser correspondence. Wetness and flooding are strongly correlated with the ratio of snow load and ice thickness while the relation to the amount of ridging is less conclusive. Using an isostatic argument, the contribution of snow ice formation to the overall ice growth was shown to be considerably higher than that of congelation ice growth. It was found that one length unit of snow accumulation or bottom ice melt on an ice floe leads to approximately the same amount of subsidence for the floe. Further, rates of subsidence, due to snow load and ice melt, appear to be similar to uplift from congelation ice growth. The degree of isostatic balance on different spatial scales was evaluated by introducing a generalized density-weighted snow/ice thickness ratio (GSI) for the drilling data. The GSI includes slush densities in order to account for the suggested importance of snow ice formation. Deviations from isostatic balance occur locally but decrease quickly on spatial averaging scales of a few meters. The closest fit to isostatic equilibrium is reached by choosing a maximum value for the slush density.

1. Introduction

The variable extent and thickness of sea ice in the south polar ocean reflects a sensitive interaction with the Antarctic climate. The most relevant property of any sea ice cover is its insulating effect on the ocean by diminishing energy exchange with the atmosphere. Oceanic heat and moisture fluxes in the Arctic regions are reduced by up to 2 orders of magnitude in the presence of a winter sea ice cover [*Maykut*, 1978]. Variations in oceanic and atmospheric temperatures as well as precipitation rates are also intricately linked to changes in the sea ice cover. In various studies [*Fletcher*, 1969; *Budd*, 1975; *Ackley and Keliher*, 1976; *Streten and Pike*, 1980; *Ackley*, 1981; *Carleton*, 1981; *Cavalieri and Parkinson*, 1981; *Gordon and Taylor*, 1975; *Gordon*, 1981; *Hibler and Ackley*,1983; *Sturman and Anderson*, 1986], evidence was found that increased energy flux through open water areas that develop within the sea ice can lead to enhanced cyclogenesis, thus affecting the atmospheric circulation and the global climate. Conversely, atmospheric temperatures and winds can influence processes like freezing, melting and transport of sea ice. Atmospheric conditions as well as sea ice growth and dynamics are mutually dependent on ocean circulation [*Jacobs and Comiso*, 1989; *Martinson*, 1994].

The climatic influence of a sea ice field is further complicated by the presence of snow cover [*Ackley et al.*, 1990; *Ledley* 1991, 1994; *Massom et al.*, 1997; *Sturm et al.*, 1998]. Snow acts as an insulator, thus keeping the sea ice warm and thin. But at the same time, snow also raises the albedo, thus leading to lower temperatures and thicker sea ice. The role of snow becomes even more ambiguous through the process of flooding [*Eicken et al.*, 1995a; *Lytle and Ackley*, 1996] which initiates brine and seawater infiltration into near-surface snow layers. Once a snow layer is flooded it freezes and snow ice forms. As field studies have proven [*Eicken et al.*,1994; *Lange et al.*, 1990] flooding and snow ice formation are widespread in Antarctica and their impact on sea ice processes is important. *Lytle and Ackley* [1996] showed that the presence of liquid water in slush during the formation of snow ice initiates convective processes that can increase the heat transfer from the base to the surface of an ice floe. This, in turn, may reduce the amount of bottom melting. Flooding also affects changes in the albedo (and hence the local radiation budget) of sea ice and alters its passive and active microwave signatures [*Drinkwater et al.*, 1993; *Hosseinmostafa et al.*, 1995]. Finally, the intrusion of seawater plays an important role in biological processes as it promotes the development of algal communities at the snow ice interface [*Fritsen et al.*, 1994; *Ackley and Sullivan*, 1994].

Compared with the Arctic, snow and ice thickness data of the Antarctic Ocean are sparse, as they are limited to drilling data to date. Detailed snow and ice measurements have been collected in the Weddell Sea [*Wadhams et al.*, 1987; *Lange and Eicken*, 1991; *Massom et al.*, 1997] and in East Antarctica [*Allison*, 1989; *Allison et al.*, 1993; *Allison and Worby*, 1994]. Between 1993 and 1995 the research vessel *Nathaniel B. Palmer* (NBP) made four voyages into the pack ice of the south polar Pacific Ocean. The two main regions that were visited are the Amundsen and Bellingshausen Seas and the Ross Sea, which represent, next to the Weddell Sea, a region of great variability in sea ice extent

[1]Now at Munich, Germany.

Paper number 98JC02414.
0148-0227/98/98JC-02414$09.00

[*Streten and Pike*, 1980]. Snow and sea ice thickness distributions in the Amundsen and Bellingshausen Seas of late winter 1993 were presented and discussed in detail by *Worby et al.* [1996]. *Sturm et al.* [1998] presented a study of snow cover properties in the Bellingshausen, Amundsen, and Ross Seas between 1994 and 1995. How the spatial distribution of snow and ice thickness and of ice structure relate to atmospheric and oceanic conditions in the early winter Ross Sea of 1995 has been shown by *Jeffries and Adolphs* [1997].

This study is based on the whole snow and ice thickness data set of all cruises that were carried out between 1993 and 1995. A synoptic and comparative presentation of the snow and ice thickness data, characterized by region, season, and year is given in section 3. The temporal and spatial characteristics of these thickness distributions emphasize the high regional importance of snow ice formation. To investigate this important growth process in more detail, freeboard and its relation to surface wetness is studied in section 4 to reveal possible differences between the potential for snow ice formation (negative freeboard) and its actual occurrence (flooding). The presence of liquid seawater in the snow cover during snow ice formation leads to the question of isostatic balance and its dependency on snow and slush densities (section 5). A new isostatic equation that includes slush density is used in section 6 to estimate isostatic depression and uplift as the result of snow loading, bottom melting, and ice growth.

2. Fieldwork and Data

Figure 1 shows ship tracks, geographical areas covered, dates, and seasons of all NBP cruises between 1993 and 1995. As can be seen in Figure 1, NBP 95-3 was an early winter Ross Sea expedition that was the first and only opportunity for the ice-breaker to enter the inner pack ice. During this cruise the ship came closest to the continent, being only 19 km away from the Ross Ice Shelf. Two fundamentally different sets of snow and ice thickness data were acquired for all these cruises.

Set A consists of ice thicknesses obtained by drilling holes at spacings of 2 m (for the 1993 and 1994 cruises) and 1 m (for the 1995 cruises) along transects that typically included 50 to 100 holes. One to three such profiles were obtained per floe. Following the method of *Worby et al.* [1996] an attempt was always made to select a floe that was characteristic of the region in which the ship was operating on that particular day. Also, transects were laid out in an effort to be representative for a given floe. Because of the common occurrence of features caused by the deformation of ice, each transect typically crossed at least one ridge or raft.

Set B is a set of snow and ice thickness measurements that were made hourly while the ship was in motion. Twenty-five visual estimates of snow and ice thickness were made once every hour for individual floe pieces that were tipped over by the ship. A buoy of known diameter, which was attached to the side of the ship, was used as a scale.

The specific sampling bias of each of the two data sets (set A and set B) has been discussed in detail by *Worby et al.* [1994, 1996] and *Jeffries and Adolphs* [1997]. The temporal bias, resulting from the fact that the ship takes some time to get across the pack, is neglected in the following study.

An overview of statistical parameters for set A and set B is given in Table 1. Some of these parameters are taken from *Worby et al.* [1996] and *Jeffries and Adolphs* [1997]. In addition to the snow and ice thickness data, qualitative data on the wetness of the snow/ice interface at each drilling location were acquired for the 1995 cruises. For all cruises, snow densities were measured at one to three sites per floe [*Sturm et al.*, 1998].

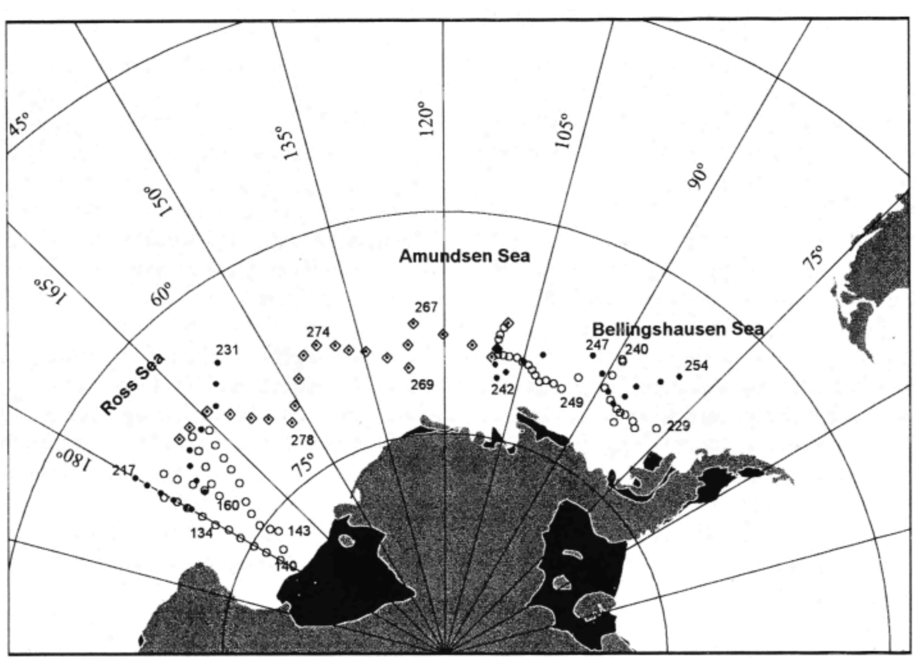

Figure 1. Ice stations along five different track lines followed by the R/V Nathaniel B.Palmer (NBP) between August 1993 and September 1995. NBP 95-3 (open circles) covered the Ross Sea in early winter (May/June 1995); NBP 95-5/1 (solid circles) covered the Ross Sea in late winter (August 1995). NBP 93 went in the Amundsen/Bellingshausen Seas in late winter 1993 (August/September 1993); NBP 95-5/2 (solid circles) revisited the same area in 1995 (August/September 1995). NBP 94 (dotted diamonds) spanned the area of the Amundsen Sea to the north- western Ross Sea in late winter (September/October 1994).

Table 1. Snow and Ice Thickness Mean Values and Standard Deviations for Data Sets A and B for all Cruises

Cruise	Ice Stations, Set A									Continuous Measurements, Set B		
	Number of Holes	Number of Floes	h_{ice}	h_{snow}	$h_{freeboard}$	Freeboard < 0	Ridging[a)]	$h_{levelice}$	$h_{ridgedice}$	Number of Observations	h_{ice}	h_{snow}
NBP 93	1142	29	88 (64)	23 (16)	2.6 (6.8)	18 (32)	62	69 (35)	98 (68)	4051	61 (27)	21 (12)
NBP 94	2235	23	84 (46)	28 (16)	-0.8 (6.0)	50 (64)	25	77 (28)	106 (73)	9673	52 (25)	16 (10)
NBP 95-3/Ro1[b)]	3670	29	65 (33)	15 (11)	1.4 (5.5)	29 (46)	34	59 (18)	76 (48)	11114	51 (27)	11 (10)
NBP 95-5/Ro2[c)]	2078	14	77 (29)	26 (12)	-0.3 (5.3)	51 (66)	25	76 (25)	77 (40)	7167	45 (27)	12 (11)
NBP 95-5/Am[d)]	2095	14	91 (69)	22 (14)	3.4 (7.4)	14 (30)	45	78 (59)	108 (75)	6949	50 (31)	13 (13)

Values are in centimeters. Standard deviations are given in parentheses. NBP is the R/V *Nathaniel B. Palmer*.

a) Negative freeboard and ridging are given in percent. Ridging, mean thicknesses for ridged and level ice in the drilling data were obtained using the Rayleigh ridge criterion.

b) early winter Ross Sea (May/June 1995).

c) late winter Ross Sea (August 1995).

d) late winter Amundsen and Bellingshausen Seas (August/September 1995).

3. Snow and Ice Thickness Distributions

3.1. Comparability and Bias of the two Methods

As addressed by *Worby et al.* [1996], the two ice thickness data sets A and B have an area of sampling overlap between roughly 0.3 to 1 m, in which they should be comparable. The following analysis justifies this in more statistical terms for the ice thickness distribution of the early winter Ross Sea cruise.

Figure 2 shows the probability density function (PDF) of the ice thicknesses measured by the two methods showing their extent of comparability. Figure 2c shows the PDF of ice thickness obtained by drilling (method A) during NBP 95-3. Figure 2a displays the corresponding distribution of ice thickness that was sampled by method B for this particular cruise.

In order to compare the results of the two methods an attempt was made to remove their respective biases. For set A a Rayleigh ridge criterion [*Wadhams and Horne*,1980; *Wadhams et al.*,1992] was applied to the data. In an analogy to *Eicken et al.* [1995b], level ice was identified for sections with a minimal length of 20 m, which were bounded where the local ice thickness departed by more than 50% from the mean thickness over the section. Using this criterion, level ice can be separated from deformed ice as shown by the shaded areas in Figure 2c. Figure 2b shows the resulting level ice PDF of the drilling data (set A). Subtraction of the thin ice bin (0-0.3 m ice) from the set B PDF in Figure 2a and recalculation of the mean and standard deviation (0.57 and 0.24 m, respectively) show a reasonably close agreement with the respective values for the level ice PDF of set A (Figure 2b).

It must be noted that the attempt to remove the biases of both methods occurred a priori and is only approximate. Even at significance levels ($\alpha<0.001$), statistical t and f tests reject the null hypothesis of equal mean and standard deviation, respectively. Due to the large sample sizes ($n > 2000$) for both data sets, their means and standard deviations should agree at the sub centimeter level for the null hypothesis to hold. Hence, the failure of the t and f tests suggests the presence of more unresolved systematic errors in one or both methods. Nevertheless, it seems reasonable to assume that most of the initial bias present in both methods was indeed removed by this simple approach. Within their region of overlap, between roughly

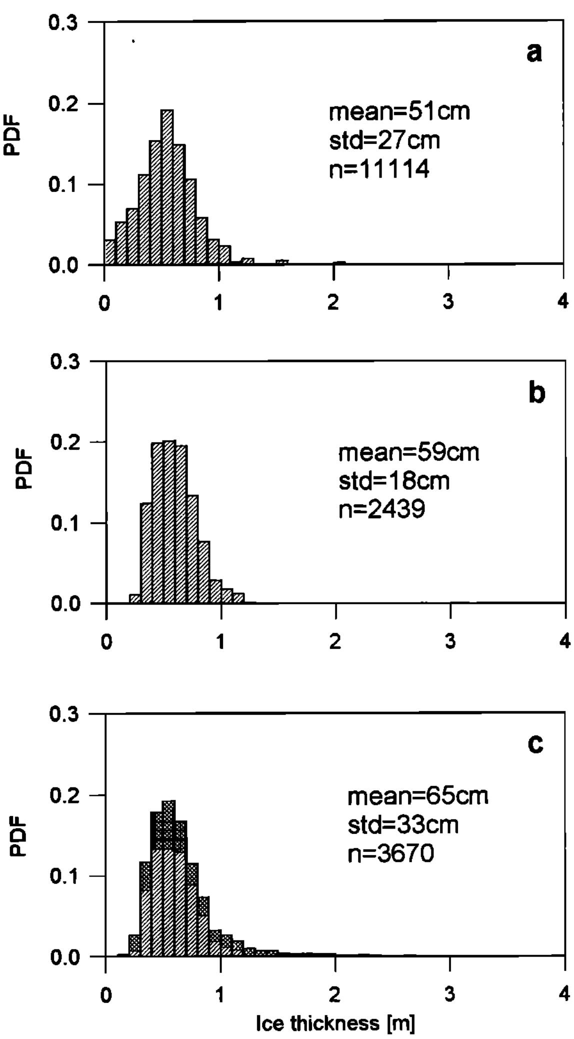

Figure 2. Probability density functions (PDFs) of ice thickness for (a) set B data, (b) set A level ice, and (c) all drilling data of NBP 95-3. Shaded areas in Figure 2c indicate the relative amount of ridging, which contributed 34% to the total distribution.

30 to 100 cm ice thickness, both methods will likely give representative estimates of the real ice thickness distribution.

3.2. Snow and Ice Thickness Data Grouped in Distance Classes

Snow and ice thickness data in two major geographical areas, the Ross Sea and the Bellingshausen/Amundsen Seas, were grouped into classes in terms of distance from the ice edge. Figure 3 is a presentation of mean sea ice and snow thickness data sorted in such distance classes for both set A and set B Ross Sea data in early (Figures 3a and 3b) and late winter (Figures 3c and 3d). Figure 4 is a similar presentation of the late winter data, which were obtained in the Amundsen and Bellingshausen Seas in 1993 and 1995. Values of standard deviations σ are given along the lines of mean snow and ice thicknesses. Standard errors ($\sigma/\sqrt{n}$) are generally 2 orders of magnitude less than all thickness values. As σ of the snow thickness distributions is slightly smaller than for the ice distributions, the corresponding errors for the former are even smaller. Errors are slightly larger for the set A data than for the set B data, since they contain fewer ice observations per distance class. A similar grouping in distance classes has been carried out by *Worby et al.* [1996] and by *Allison and Worby* [1994] for East Antarctic snow and ice. It is important to note that each distance class contains all data of its specified range of distances from the ice edge. In this way, each distance class averages both in the zonal and (to a lesser extent) in the meridional dimension.

For both data sets (set A and set B) of the Ross Sea in early winter (Figures 3a and 3b) one can clearly discern three characteristic zones, which were defined by *Jeffries and Adolphs* [1997] for set A. The first zone is the area in the vicinity of the continent at >1200 km from the ice edge where the mean ice thickness is low. The second zone between 800 and 1200 km from the ice edge consists of thick ice for both sets A and *B* (Figures 3a and 3b). Zone 3 (<800 km from the ice edge) is characterized by a distinctly lower mean ice thickness that declines toward the ice edge. Absolute values of ice and snow thickness are higher for the drilling data (Figures 3a and 3c) than for the shipboard measurements (Figures 3b and 3d), but the tendency of relative variability with space is similar for both sets of each cruise. The graphs for the late winter Ross Sea (Figures 3c and 3d) cover only the distances between 0 and 800 km, but they show the same trend as zone 3 of Figures 3a and 3b for the early winter cruise. The distance class between 0 and 200 km (zone 4) from the ice edge appears only in the Set B data (Figures 3b and 3d) and shows distinctly lower ice and snow thicknesses than in zone 3.

During late winter sea ice conditions also restricted the research vessel to the outer pack ice (< 800 km from the ice edge) in the Amundsen and Bellingshausen Seas (Figure 4). As in the Ross Sea (Figure 3), there is a general increase in ice thickness from the ice edge toward the continent. However, contrary to the data from the Ross Sea where different distance classes are similar for set A and set B, the trend of thickening toward the continent in the Bellingshausen and Amundsen Seas is much more pronounced for the drilling data than for the continuous observations (Figures 4c and 4d). Since the 1993 cruise in the Amundsen and Bellingshausen Seas covers only the relatively small area between 50 and 450 km from the ice edge, it is difficult to make comparisons between distance classes. As in the Ross Sea, there is also a distinct class of thin ice with thin

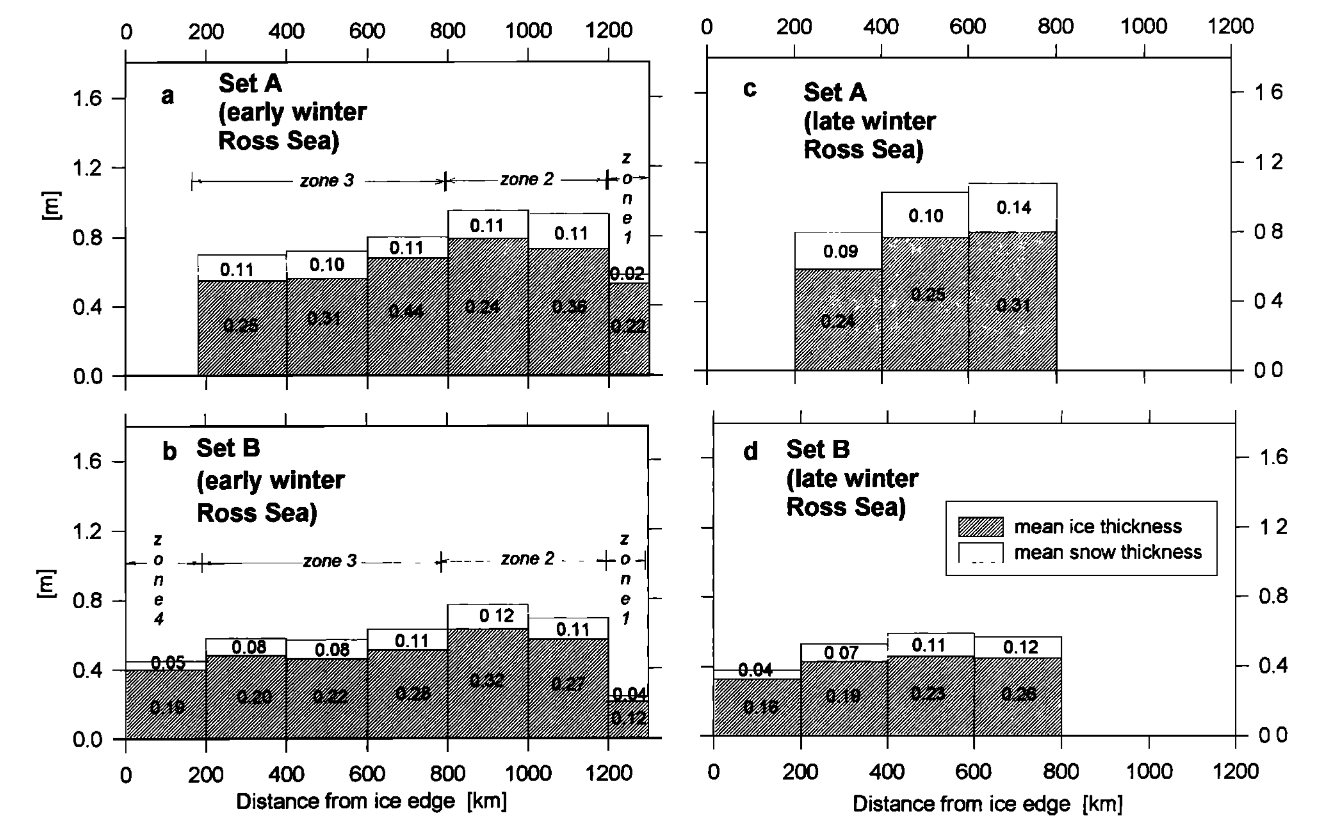

Figure 3. Mean values of ice thicknesses and snow depth sorted in distance classes from the ice edge for (a) set A and (b) set B data of the early winter Ross Sea cruise and for (c) set A and (d) set B data of the late winter Ross Sea cruise. Corresponding standard deviations are indicated as numbers (in meters).

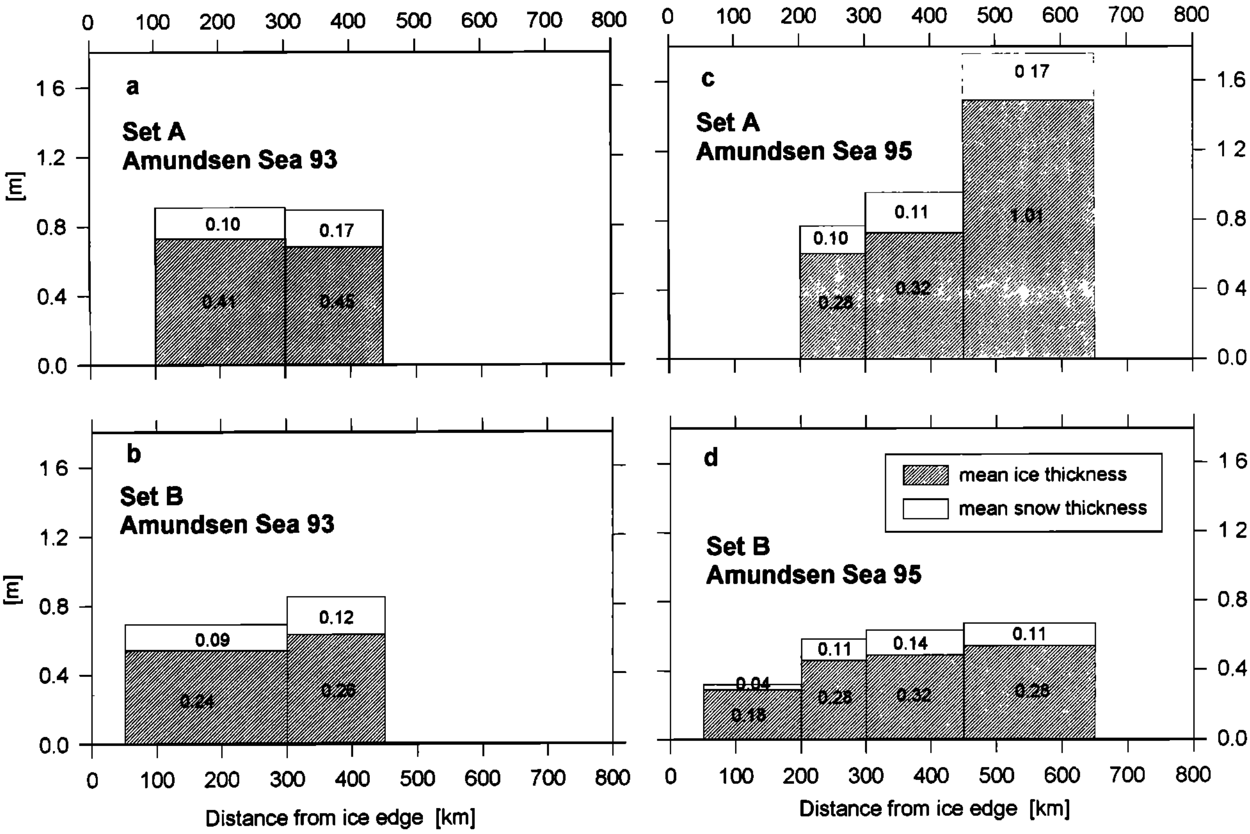

Figure 4. Mean values of ice thicknesses and snow depth sorted in distance classes from the ice edge: (a), (b) for Set A and Set B data of the Amundsen and Bellingshausen Seas in late winter 1993, (c), (d) in in late winter 1995. Corresponding standard deviations are indicated as numbers (in [m]).

snow cover in the set B data (Figures 4b and 4d) for the Bellingshausen/Amundsen Seas at distances <200 km from the ice edge. In the classes >200 km, the set A data contain higher mean ice and snow thickness values than set B data (Figures 4c and 4d) as well as a more pronounced increase toward the continent, especially in the class >450 km. This pattern of greater difference between set A and set B in the Amundsen and Bellingshausen Seas can also be seen in Table 1.

3.3. Seasonal Comparison of Distance Classes in the Ross Sea

As discussed in detail by *Jeffries and Adolphs* [1997] the steep decline toward a very small mean ice thickness for *set A* of the early winter Ross Sea (zone 1 in Figure 3a) gives evidence of the fact that ice production takes place in near coastal polynyas and leads. From its origin near the continent, the thin ice drifts then away toward the interior pack ice zone, where it thickens by deformation and thermodynamic growth (zone 2). As further shown by *Jeffries and Adolphs* [1997], the marked difference in ice thickness between zones 2 and 3 can be explained by a combination of oceanographic and atmospheric influences. The trend of similar relative variability with distance for both sets A and B, seen in Figure 3 a and b, can be taken as proof of the general comparability (section 2) of the two methods despite the difference in sampling range. An exception is the thin ice zone (zone 4) which only shows up in set B (Figures 3b an 3d) and represents young ice near the ice edge consisting of pancakes and small cake floes.

The graphs of the late winter Ross Sea cruise (Figure 3c, d) include only observations between 0 and 800 km from the ice edge, which can be compared to zone 3 of the early winter cruise. Despite the 3 month time gap, there are no marked differences between the changes in snow and ice thickness in the set B data of the late winter Ross Sea in comparison to the 0-800 km zone of the early winter Ross Sea. Both continuous data sets B from the Ross Sea display a strikingly similar, seasonally independent pattern in the common zone of overlap from 0 to 800 km distance from the ice edge. A comparison of the drilling data (set A) in their zone of overlap (200-800 km) shows slightly higher ice and snow thickness values for the late winter set (Figures 3a and 3c). This shows that medium to large ice floes that are suitable for drilling are thicker later in the season (see also Table 1). Since this thicker ice does not fall in the sampling range of the shipboard measurements, it is not reflected in set B.

3.4. Distribution Functions of Ice and Snow Thicknesses and Freeboard

Since the two Ross Sea cruises made it possible to study the same area twice within 4 months in 1995, it is useful to define a common geographic area (between 64.87° and 70.62° southern latitude) where the two cruises overlapped. The drilling data for this common area are shown in Figure 5. Since the latitudinal band covered by the early winter data set is larger than the defined common geographic area, Figure 5 contains all the drilling data of late winter but only those parts of the set A data for early winter which were sampled in the common area. It is clear that there is a tendency for the snow and ice PDFs to

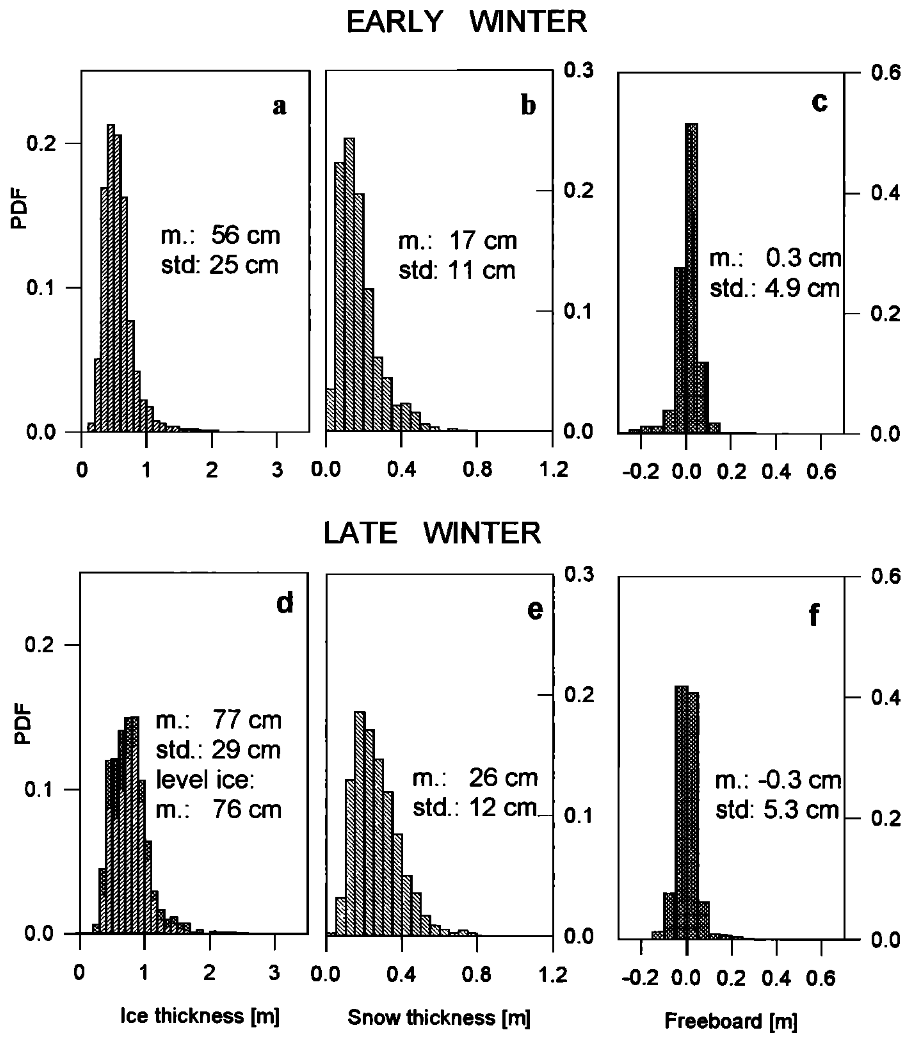

Figure 5. Probability density functions (PDFs) of drilling data (set A) for the (a)-(c) early and (d)-(f) late winter Ross Sea cruises in their common area of overlap between 64.87°S and 70.62°S. Darker areas in Figure 5d indicate the contribution of ridging for the late winter Ross Sea.

become flatter and to shift toward higher thickness values later in the season. Mean snow and ice thickness values are also larger in late winter, and there is a slight increase in the variance. A comparison between the two freeboard distributions (Figures 5e and 5f) shows a considerable number of freeboard measurements in the 0 to 5 cm bin in early winter and a larger number of negative than positive freeboard values in late winter.

Figure 6 shows PDFs of the drilling data for the Bellingshausen and Amundsen Seas in 1993 and 1995. Data from the 1994 cruise are also included for comparison. Shaded areas indicate the amount of ridged ice in each particular ice thickness bin. One sees that deformation plays a much greater role in the Bellingshausen and Amundsen Seas (Figures 6a and 6b) as compared to the late winter Ross Sea (Figure 5d) and to cruise 94 (see also Table 1). The PDFs for the Bellingshausen and Amundsen area are broader and shifted toward larger ice thicknesses (Table 1) as compared to both the Ross Sea (Figure 5d) and to NBP-94 (Figure 6c). Furthermore, they exhibit a more irregularly shaped appearance that is shared with the ice distribution of NBP-94.

Figure 7 shows a comparison of set B PDFs between the Amundsen and Bellingshausen Seas (Figures 7a-7c) and the Ross Sea (Figures 7d-7f) in late winter 1995. In addition to showing slightly higher mean values for the Amundsen Sea, the most obvious difference between the two geographical areas appears to be the shape of the PDFs with the distribution functions being more irregularly shaped in the Amundsen Sea as compared with the Ross Sea.

3.5. Distribution Functions of Drilling Data

The increase in ice thickness shown in Figures 5a and 5d is undoubtedly due to the fact that by late winter, sea ice has had more time to grow thermodynamically and to show thickness increases resulting from mechanical deformation than in early winter. An increase in snow thickness follows since older ice has also had more time to accumulate snow. A comparison between freeboard PDFs (Figures 5c and 5f) shows that a high flooding potential apparent in early winter (bin 0-5 cm) has been realized in late winter. The increase in flooding may be due to the proportionately greater increase in snow thickness as opposed to ice thickness later in winter.

The drilling PDFs for the Bellingshausen and Amundsen Seas (Figures 6a and 6b) show long tails, extending to larger ice thicknesses. It has been suggested [*Worby et al.*, 1994; *Jeffries et al.*, 1994] that deformation plays an important role in the Bellingshausen and Amundsen Seas. Therefore the tails of the

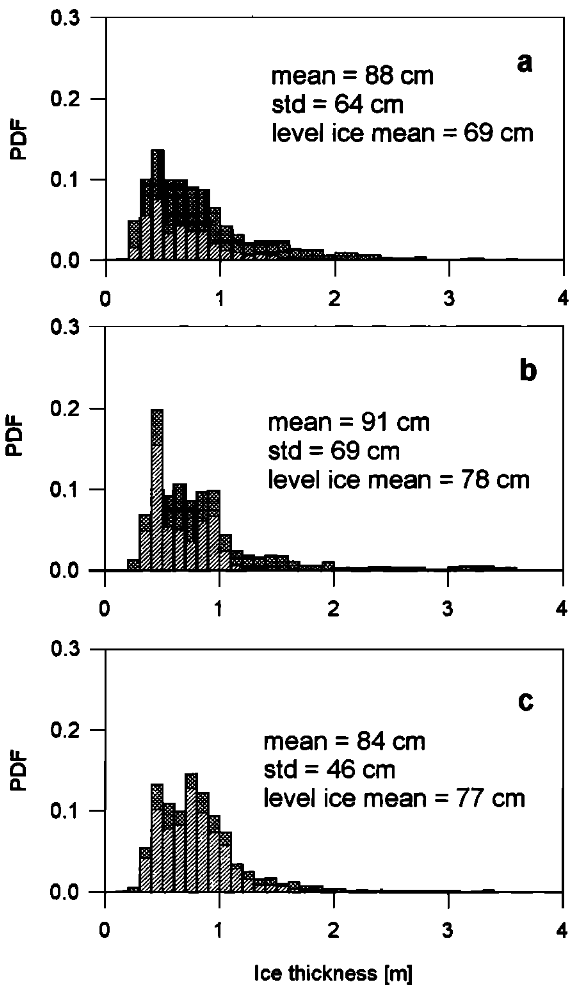

Figure 6. Probability density functions (PDFs) of ice thickness of the drilling data (set A) for the Amundsen and Bellingshausen Seas in (a) 1993, (b) 1995, and (c) for cruise NBP 94. Means, standard deviations (std), and mean level ice thicknesses are also indicated. Shaded areas show the contribution of ridging in the respective areas.

distribution functions in Figures 6a and 6b can be interpreted as indicative for deformation. The two Ross Sea areas (Figures 2c and 5d), which are clearly less ridged than the ice in the Amundsen and Bellingshausen Seas (see also Table 1), also show distinctly less flattened and more symmetrical ice thickness PDFs. The ice thickness distribution for cruise 1994 shows a mixture of Amundsen and Bellingshausen and Ross Sea characteristics. Like the Ross Sea distribution, it shows less ridging and a confined range of ice thicknesses and like the distributions of the Amundsen and Bellingshausen Seas, it is more irregularly shaped and shows a large mean ice thickness value.

4. Floe Freeboard, Surface Wetness and Isostatic Balance

4.1. Investigations of Flooding Prior to and After Drilling: Spatial and Seasonal Differences

The analysis in section 3 suggests indirectly that much of the negative freeboard measured in the early season has caused significant later growth of snow ice via flooding. This poses the interesting question of how much negative freeboard and flooding (with subsequent snow ice formation) are closely related. To address this issue, all drilling locations of the 1995 cruises were qualitatively examined prior to drilling and classified, according to an ascending degree of wetness, as dry, moist, wet, or slushy. In this characterization, only the slushy locations indicate standing water and therefore qualify as flooded prior to drilling. The results of this examination will be presented in the following section in order to study the relation between the degree of wetness before drilling and the freeboard after drilling. In this analysis the influence of the field party and its activities on the measurements may be a nonnegligible factor. For that reason an upper limit of this influence has been calculated, treating the ice floe as a two-dimensional elastic plate [*Parmerter*, 1974]. For typical first-year ice (Young's modulus 3×10^4 N cm^{-2}, Poisson ratio 0.3) of 40 cm thickness and a 25 person field party, uniformly distributed along a 50 m line, a maximum deflection of 1.6 cm was obtained. It can be concluded that, considering typical freeboard values of -1 to +3 cm, the field party can have a noticeable impact on the locally measured freeboard.

4.2. Freeboard Statistics of the Wetness Groups and Processes Affecting it

Figure 8 shows the freeboard distribution functions for the early winter Ross Sea cruise, the late winter Ross Sea cruise, and the late winter Amundsen Sea cruise for all wetness groups. Wetness increases in descending order from dry to slushy (or flooded) locations.

In this investigation, group 3 (slushy and/or flooded) shows the most obvious results (Figures 8j-8l). Most locations that were flooded or slushy had negative freeboards after drilling. In the late winter Ross Sea, not a single positive freeboard was measured at any location belonging to group 3, whereas in the early winter (Figure 8j) and in the Amundsen Sea (Figure 8l) a few positive freeboards were observed. Negative freeboards also dominate the moist and wet groups (groups 1 and 2, Figures 8d-8i). The only exception is the moist group of the late winter Amundsen Sea, where only 45% of the freeboards were equal or below zero.

Even locations that were dry prior to drilling show a substantial number of cases where freeboards were at or below zero (Figures 8a-8c). For example, up to 25% of the freeboard measurements from the Ross Sea during late winter were negative and an additional 20% were zero. Negative freeboard could have been caused by the weight of the field party. Another possibility is that sea water incursion into the snow layer was reduced owing to the low permeability of the underlying ice [*Massom et al.*,1997; *Eicken et al.*, 1994].

Less than 5% of the freeboards observed at flooded locations (group 3) were positive. However, the number of positive freeboards within the moist and wet groups (groups 1 and 2) was seen to be generally not negligible (Figures 8d-8i). Group 2 (wet locations) shows a maximum contribution of 12% positive freeboard (Figure 8i). About 20% positive freeboards seems to be characteristic for the moist group (group 1); the Amundsen Sea even showed a contribution of 55% positive freeboards. At these locations, where the ice surface is above the water level, water could have entered as a result of a number of processes. Brine or seawater could have been expelled upward through the brine channels into the snow cover on top of the ice surface [*Perovich and Richter-Menge*, 1994; *Massom et al.*, 1997; *Lytle and Ackley*, 1996]. Further, small cracks, mostly formed as a by-product of ice deformation, could serve as openings for seawater to be sucked into the snow cover by capillary pressure [*Massom et al.*, 1997].

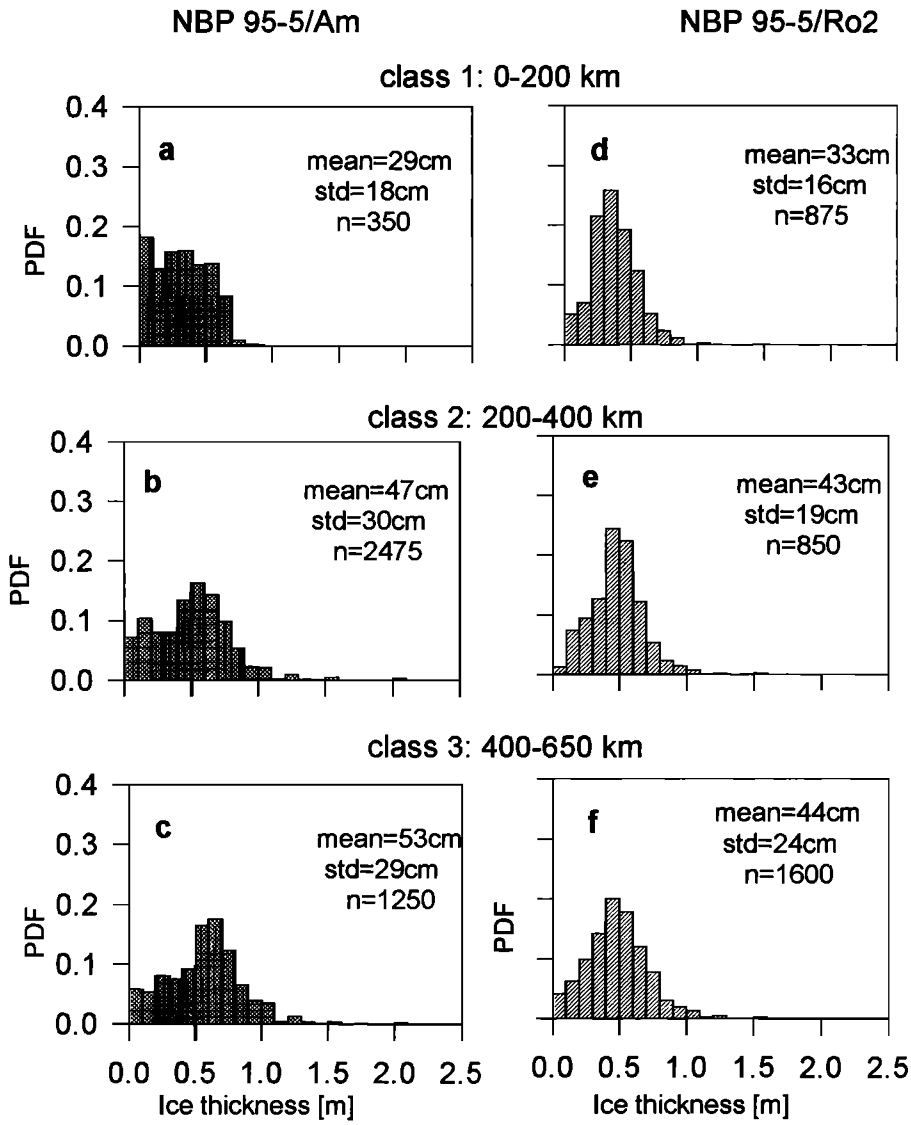

Figure 7. Probability density functions (PDFs) of ice thickness of the continuous shipboard measurements (set B) for the (a)-(c) Amundsen and Bellingshausen Seas and (d)-(f) Ross Sea in late winter 1995, sorted in three, common distance classes from the ice edge. Mean values, standard deviations (std), and numbers of observations (n) are indicated in the graphs.

The occurrence of high-salinity pockets in the snow above the level of flooding confirms the importance of these processes [*Sturm et al.*, 1998, *Massom et al.*, 1997].

Figure 8 also shows some correspondence between the degree of wetness to the snow/ice thickness ratio, and a less conclusive relation to the percent ridging (see numbers given in Figure 8). Snow-to-ice thickness ratios become progressively greater as the degree of wetness increases. A larger amount of ridging is related to a higher degree of moisture for the early winter Ross Sea, but there is an opposite trend for the late winter Ross Sea. Some slight anticorrespondence between these two variables is also seen for the Amundsen and Bellingshausen Seas. That ridging seems to reduce the overall percentage of negative freeboard values observed can be seen in Table 1, where areas with little ridging such as the Ross Sea in late winter show the highest percentages of negative freeboards (51%). This fact could be explained by the observation that the load distribution of keel and sail causes depression of the ice sheet adjacent to the ridge, thus inducing flooding, while the ridge itself is strongly uplifted

It can be concluded that there is effectively a 1 to 1 correspondence between flooding and negative freeboard (results of group 3), with an uncertainty of up to 5%. The correlation is still fairly good for locations that were identified as wet prior to drilling which showed only 5 to 10% of positive freeboard. If one tries to correct for a possible people deflection (see previous section), an offset of 1.6 cm, at the most, could be effected in the freeboard statistics of Figure 8. However, the above interpretation of the freeboard statistics in relation to wetness would remain generally unchanged.

4.3. Isostatic balance: Relationship between sail and keel

Knowledge of the relationship between sail and keel distributions is especially useful to complement measurements with only one of the distributions being available. Establishing such a relationship should be the easier, the more isostatically balanced the floes are. As indicated in section 4.1 and 4.2, deformation (ridging and rafting) plays an important role in determining the characteristics of the snow and sea ice thickness

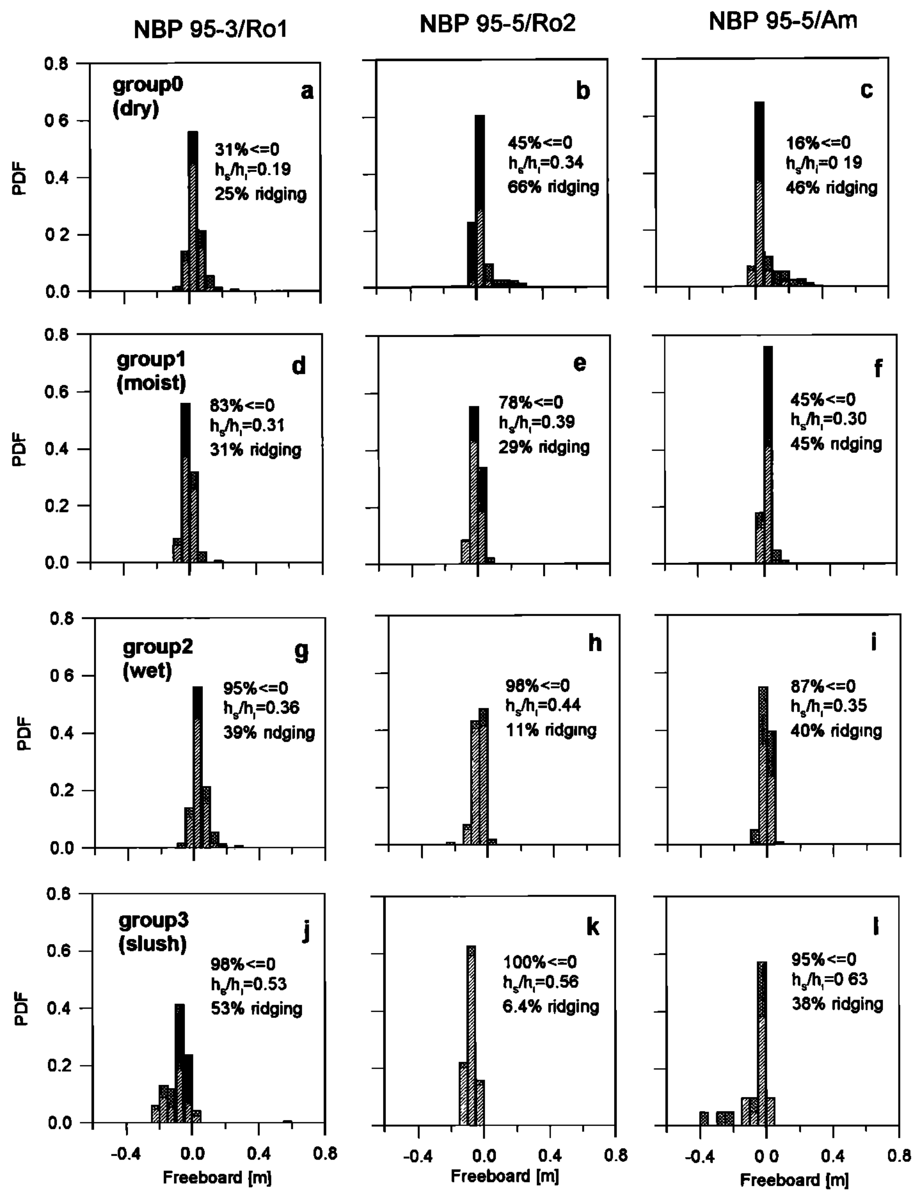

Figure 8. Probability density functions (PDFs) of freeboard for the (left) early winter Ross Sea, (middle) late winter Ross Sea, and (right), the late winter Amundsen and Bellingshausen Seas in 1995, sorted into groups of different degree of moisture prior to drilling. (a)-(c) Group 0, indicates dry locations; (d)-(f) group 1 moist locations; (g)-(i), group 2, wet locations; and, (j)-(l), group 3, locations, which were detected as slushy of flooded. The relative amount of zero or negative freeboard (in percent), mean snow/ice thickness ratios, and the contribution of ridging (darker areas) are also indicated in the corresponding graphs.

distribution. The contribution of ridged ice to the total measured sea ice in the drilling data (set A) was determined using the Rayleigh ridge criterion [*Eicken et al.*, 1995b; *Wadhams and Horne*,1980; *Wadhams et al.*,1992], and the percentages are given in Table 1. For Arctic sea ice it was found [*Weeks et al.*,1980; *Wadhams and Horne*,1980; *Wadhams et al.*,1992; *Comiso et al.*,1991] that sail and keel thickness distributions of sea ice, selected with the Rayleigh ridge criterion, obey a negative exponential distribution of the form

$$n(h)dh = A_{sa/ke} \exp(-a_{sa/ke} h)dh \qquad (1)$$

where $n(h)$ is the probability that the thickness value h lies between h and $(h+dh)$. The amplitude A and the decay parameter a are parameters characteristic of the ice regime and the subscripts *sa* and *ke* refer to sail or keel. It has also been observed by *Dierking* [1995] that best fits to ridge height distributions of Antarctic sea ice are also achieved by negative exponentials.

When the sail and keel distributions of the ridged ice for the entire drilling data set of each of the cruises were fitted to (1), the values for the parameters [A,a] in Table 2 were obtained. The fit to (1) was very similar for all data sets with standard errors of 1 to 2 orders of magnitude smaller than the amplitude and generally smaller by 2 orders of magnitude than the decay parameter. Figure 9a shows a strong linear correlation (r=0.99) between the amplitudes and the decay parameters for the keel distributions of the different cruises. A positive correlation was found between the two amplitudes A_{sa} and A_{ke}, and a strongly linear correlation between the two decay parameters a_{sa} and a_{ke}

Table 2. Decay Parameters a and Amplitudes A of an Exponential Fit for the Sail (sa) and Keel (ke) Distributions of All Cruises

Cruise	Sail		Keel		R [a)]
	A_{sa}	a_{sa} m^{-1}	A_{ke}	a_{ke} m^{-1}	$\frac{\langle h_{ke} \rangle}{\langle h_{sa} \rangle}$
NBP 93	1.04	5.23	0.28	1.63	3.27
NBP 94	1.05	5.24	0.25	1.51	3.16
NBP 95-3/Ro1 [b)]	1.43	7.55	0.65	2.65	3.79
NBP 95-5/Ro2 [c)]	2.09	7.17	0.63	2.44	2.98
NBP 95-5/Am [d)]	2.00	6.77	0.48	2.01	3.49

[a)] R is the factor for a scale transformation which converts from sail to keel distribution..

[b)] Data are from early winter Ross Sea (May/June 1995).

[c)] Data are from late winter Ross Sea (August 1995).

[d)] Data are from late winter Amundsen and Bellingshausen Seas (August/September 1995).

can be seen in Figure 9b (r=0.97). A strongly linear relationship between the decay parameters, found also for Arctic sea ice [*Wadhams et al.*,1992], probably indicates that the underlying physical processes that create sail and keel are the same. Also, in comparison to Arctic values, the Antarctic amplitudes A presented here seem to be generally lower and decay parameters a are higher.

The generally good correlation between top and bottom parameters suggests that it should be possible to develop a useful transfer function between the sail and keel distributions. The practical value of obtaining such a transfer function is evident since it would allow one to measure sail profiles of large sea ice areas with a laser altimeter and then use these to derive keel distributions. This would be especially useful for future sea ice sampling in Antarctica, where submarine data are not available and drilling data are sparse and difficult to attain. *Comiso et al.*[1991] and *Wadhams et al.*[1992] have successfully developed such a transformation suitable for regions of the Arctic, where sonar as well as lidar data were available. It was accomplished by making a scale transformation on the sail distribution with the density ratio

$$R = \frac{\rho_m}{\rho_w - \rho_m} \tag{2}$$

where ρ_w is the near-surface seawater density and ρ_m is the mean density of the snow and ice. It further can be shown [*Wadhams et al.*,1992] that R equals the ratio of mean keel depth to mean sail height.

Table 2 shows the values for R for the different cruises. It can be seen that they vary with geographic region and time and range from 2.9 to 3.8, whereas typical values of R for the Arctic range between 7.2 and 8.7 [*Comiso et al.*,1991; *Wadhams et al.*,1992], again dependent on the specific region. This shows that surface features are still enhanced on the underside of Antarctic ice but by about a factor 2 less than in the Arctic. The difference in R between the Arctic and Antarctica could also reflect the different sampling methods used for the two regions. Laser and submarine sonar, used in the Arctic, sample thicker ice and more ridges as compared to the drilling data over 100 m, which are usually obtained in Antarctica. Figure 10a shows the keel distribution resulting from a sail transformation with factor R in comparison to the measured keel transformation for the drilling data of the second Ross Sea cruise (NBP 95-5). The agreement is close, with the transformed keel PDF being only slightly broader and flatter than the measured PDF. This tendency was generally observed for all cruises.

4.4. Isostatic balance: thicknesses on different scales

In order to further investigate the correlations between the different snow and ice thickness variables, values were calculated on different spatial scales. To access different spatial scales, the thickness profile f_j was averaged using Gaussian filters of the form

$$G_{i\,j} = \frac{1}{\sqrt{2\pi\tilde{n}}} \exp\left[\frac{(i-j)^2}{2\tilde{n}^2}\right],$$

where $\tilde{n} = \sigma/\Delta x$ defines the Gaussian width σ in terms of the spacing $\Delta x = 1$ m. A spatially averaged profile $\tilde{f}_i$, over the width

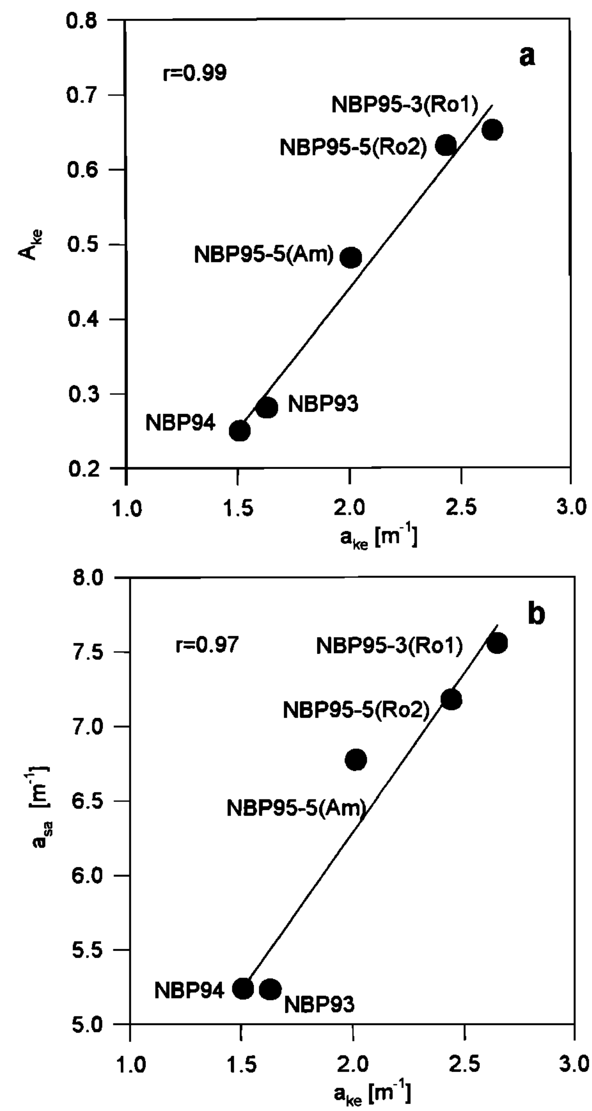

Figure 9. Linear fits (a) between underside amplitudes A_{ke} (ke denotes keel, sa denotes sail) and decay parameter a_{ke} and (b) between decay parameters of sail and keel distributions. Amplitudes and decay parameters are given for the entire data set of each cruise.

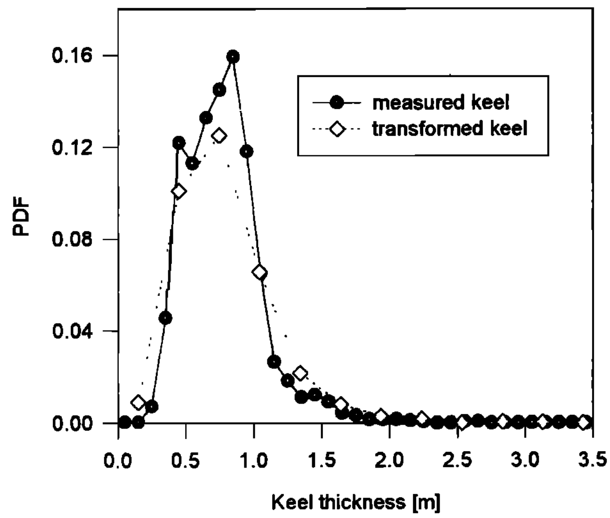

Figure 10. Results of a scale transformation with factor R for all data of the late winter Ross Sea cruise. The transformed sail distribution (diamonds) is compared to the measured keel distribution (circles).

$\tilde{f}_i$, is hereby obtained from the original profile surface f_j by

$$\tilde{f}_i = \sum_j G_{ij} f_j \ .$$

It thus was consecutively averaged over widths of 1, 2, and 5 m and over the total profile length (about 100 m).

As a general outcome of this correlation analysis, three major coefficients of significant correlations ($|r|>0.5$) could be identified. First, there was a high correlation ($|r|>0.9$) between ice and keel thickness. Second, there was a significant positive correlation between sail and keel thickness, and third, there was a negative correlation between the ratio of snow/ice thickness and the freeboard. All these correlation coefficients generally increased with averaging over larger spatial scales (such as going from the local or unaveraged scale to scales of 2, 5 m, or the total length of the profile). Most interesting in the relation of isostacy to freeboard (or flooding) is the anticorrelation between snow/ice thickness ratio and freeboard. First, it also should be noted that these anticorrelations between the snow/ice thickness ratio and freeboard improved with averaging, whereas anticorrelations between just snow and freeboard remained low (mostly distinctly lower than 0.3). This indicates that in accordance with the isostatic relationship it is not snow load in itself that determines positive or negative freeboard and hence flooding but, rather, the ratio of snow to ice thickness.

In order to further illustrate the behavior of the anticorrelation between snow to ice thickness and freeboard, hence the relation of isostacy to flooding, freeboard is graphed versus the snow/ice thickness ratio for all measurements of the two Ross Sea cruises in Figures 11a and 11d. Analogous to the study by *Massom et al.*[1997] in the Weddell Sea, these graphs can be used to examine the extent to which flooding is connected with isostatic imbalance and how this connection depends on the scale of observation. The same sets of data that are presented without averaging in Figures 11a and 11d are shown on scales of 2 and 5 m in Figures 11b, 11e and 11c, 11f, respectively.

The flooding criterion, derived from the isostatic balance equation [*Ackley et al.*,1990; *Eicken et al.*,1994], is

$$\frac{h_s}{h_i} \geq \frac{\rho_w - \rho_i}{\rho_s} \ , \qquad (3)$$

where ρ_w is the density of seawater (1.03 g cm^{-3}) and ρ_i is the density of sea ice (0.91 g cm^{-3}). As can be seen, for a certain ratio of snow to ice thickness, the occurrence of negative freeboard is mainly dependent on snow density ρ_s . The arrows in Figure 11 indicate the snow/ice thickness ratio that equals the right-hand side of (3), with the mean value of snow density measured for the each corresponding cruise. The maximum possible spread around this mean snow density is indicated by dashed straight lines at snow/ice thickness values 0.6 (corresponding to a lower bound for the density of about 0.20 g cm^{-3}) and 0.17 (corresponding to an hypothetical upper bound for the density of 0.70 g cm^{-3}). It should be noted that the choice of an upper bound for the density includes a fundamental problem. In the case of just dry or moderately wet snow the chosen value of 0.70 g cm^{-3} might be too high. However, in the case of flooded snow or slush, found at many locations, 0.70 g cm^{-3} was probably still too low for an upper bound (see section 5). The two hatched areas mark possible imbalances where the freeboard is dominated by deformation (possibly associated with ridging or rafting) rather than by isostatic load. In the first area, A_1, snow densities higher than 0.70 g cm^{-3} would be required in order to induce flooding. In the second area A_2 the snow density had to be smaller than 0.20 g cm^{-3} in order to not induce flooding.

As can be seen in Figures 11a and 11d, the number of points that are isostatically imbalanced on a local, unaveraged scale is small but not negligible. Averaging on larger spatial scales of 2 and 5 m (Figures 11b, 11d and 11e, 11f) shows that the imbalance areas A_1 and A_2 quickly become more and more depleted of points.

It therefore follows that although isostatic imbalance does occur locally, it quickly disappears when spatial averaging of only a few meters is applied. Hence it can be concluded that deformation most often does not change the isostatic balance on a scale of 2 to 5 m and, in many cases, not even on a local (or unaveraged) scale.

5. Spatial and Seasonal Differences Revealed by Examination of Isostatic Balance

5.1. Formulation of a more Generalized Isostatic Equation and its Validity for the Different Geographical Areas

In section 4, relationships between different thickness variables were examined. From the frequent occurrence of negative freeboards (Table 1) and the presence of liquid seawater in the snow cover, it became clear that a single snow density may be inadequate to describe the sea ice cover isostatically. To cure this deficiency, an isostatic equation is developed that includes the density of slush (flooded snow), in addition to the usual snow and ice densities. From this a density-weighted, "generalized" snow to ice thickness ratio will be derived which more accurately describes the problem of isostatic balance. Depending whether freeboard is positive or not one obtains for the isostatic equation

$$\rho_s h_s + \rho_i h_i = \left(h_i - h_{fb}\right)\rho_w, \quad h_{fb} \geq 0 \quad (4a)$$

$$\rho_s\left(h_s + h_{fb}\right) + \rho_i h_i - \rho_{sl} h_{fb} = \left(h_i - h_{fb}\right)\rho_w, \quad h_{fb} \leq 0 \quad (4b)$$

with freeboard h_{fb} and slush density ρ_{sl}. It should be noted that the snow thickness h_s includes h_{fb} for the case of negative freeboard that is given in (4b). The generalized ratio of density-weighted snow/ice thickness (GSI) for the two cases in (4) shall be defined as

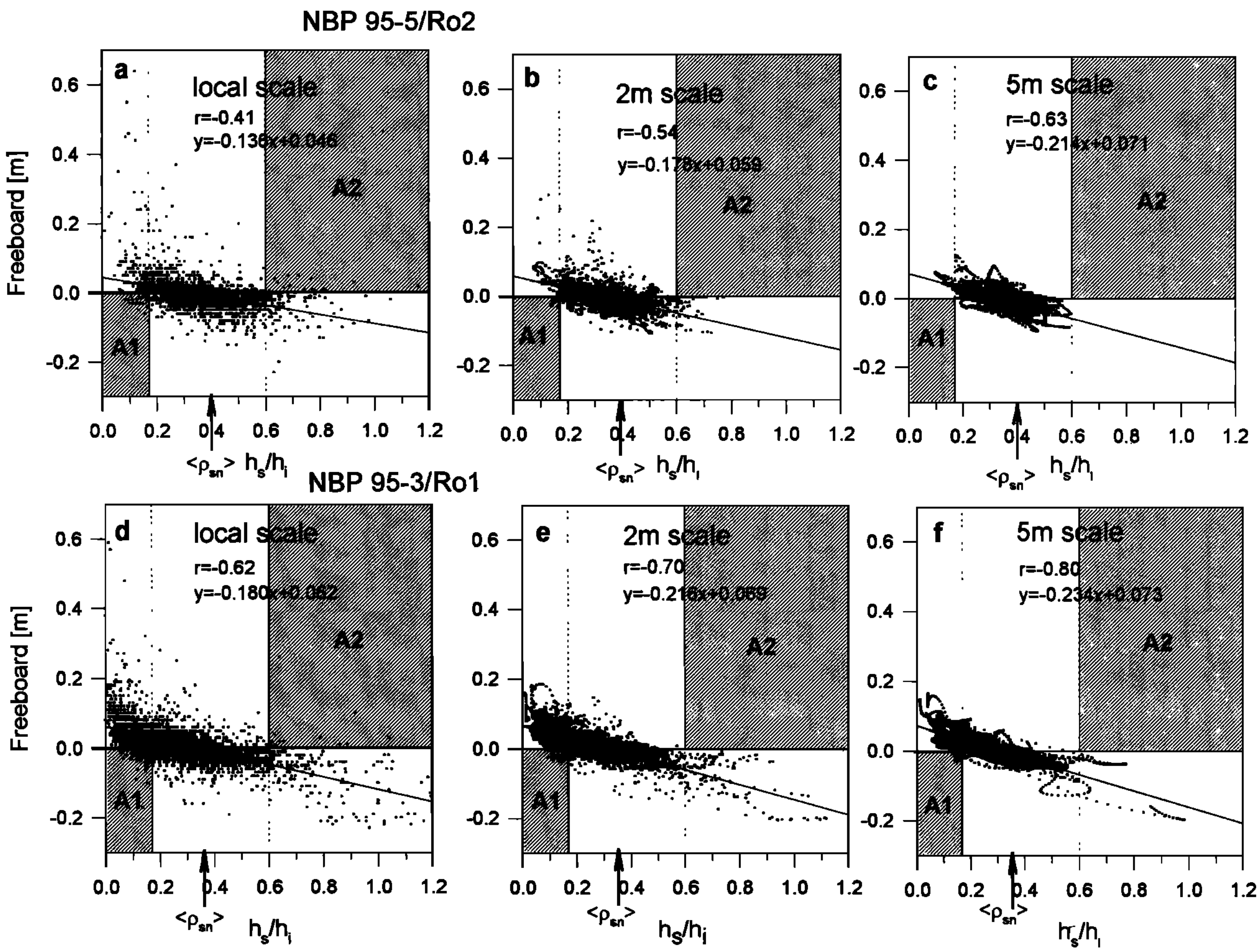

Figure 11. Snow/ice thickness ratios graphed versus freeboard for the (a)-(c) late winter Ross Sea and (d)-(f) early winter Ross Sea in 1995. The scale of averaging advances from left (local or unaveraged scale for Figure 11a and 11d, to right (2 m average in b and e, 5m average in c and f). The region within the two dotted lines refers to snow/ice thickness values that correspond to a maximum snow density range of 0.20 to 0.70 g cm-3. The hatched areas A1 and A2 indicate the two regions of isostatic instability. Arrows point to the minimal snow/ice thickness value that leads to flooding for the corresponding mean snow density of the cruise. Correlation coefficients and regression lines and their equations are shown in the graphs.

$$\mathrm{GSI} = \frac{\rho_s h_s}{\rho_i h_i}, \qquad h_{fb} \geq 0 \qquad (5a)$$

$$\mathrm{GSI} = \frac{\rho_s\left(h_s + h_{fb}\right) - \rho_{sl} h_{fb}}{\rho_i h_i}, \qquad h_{fb} \leq 0 \qquad (5b)$$

Eliminating the snow and slush densities with (4), this GSI gives, for both cases, a straight line with the freeboard/ice thickness ratio as variable,

$$\mathrm{GSI} = \left(\frac{\rho_w}{\rho_i} - 1\right) - \left(\frac{\rho_w}{\rho_i}\right)\left(\frac{h_{fb}}{h_i}\right) \qquad (6)$$

Assuming constant values for ρ_i (about 0.9 g cm^{-3}) and ρ_w (about 1.0 g cm^{-3}) isostatic balance or imbalance of a floe can be investigated by how much individual points in (5), with given snow and slush densities, deviate from the isostatic line given in (6).

Figure 12a shows the GSI plotted versus the freeboard/ice thickness ratio for all measured drilling points of the early winter Ross Sea cruise (NBP 95-3). At each drilling location, h_s, h_i, and h_{fb} were measured and used to compute the GSI values. For ρ_s the mean bulk snow density was used for the corresponding cruise. Owing to difficulties in measuring ρ_{sl}, a value of 0.70 g cm^{-3} was assumed.

The dotted line in Figure 12a is a least squares regression line for the data points. It can be compared to the isostatic line (equation (6)) in Figure 12a (solid line). However, in comparison to the local scale graphs in Figure 11, the overall scatter seems to be less in the data of Figure 12a; the regression line in Figure 12a fits the data with a correlation of 0.8. The difference between the regression line and the isostatic line can be used as a measure of how well the isostatic equation is satisfied by the data. Figure 12b shows the data of Figure 12a averaged on a 5 m scale. The correlation between the points has increased to 0.9, and there is less scatter. At the same time the regression line has approached the isostatic line. The improved fit between these two straight lines is hereby mainly caused by a better representation of the more extreme data points (GSI > 0.3) rather than a significant increase of the correlation coefficient. The latter is biased by clustering of many data points in the x range between 0.2 and -0.2 (GSI < 0.3).

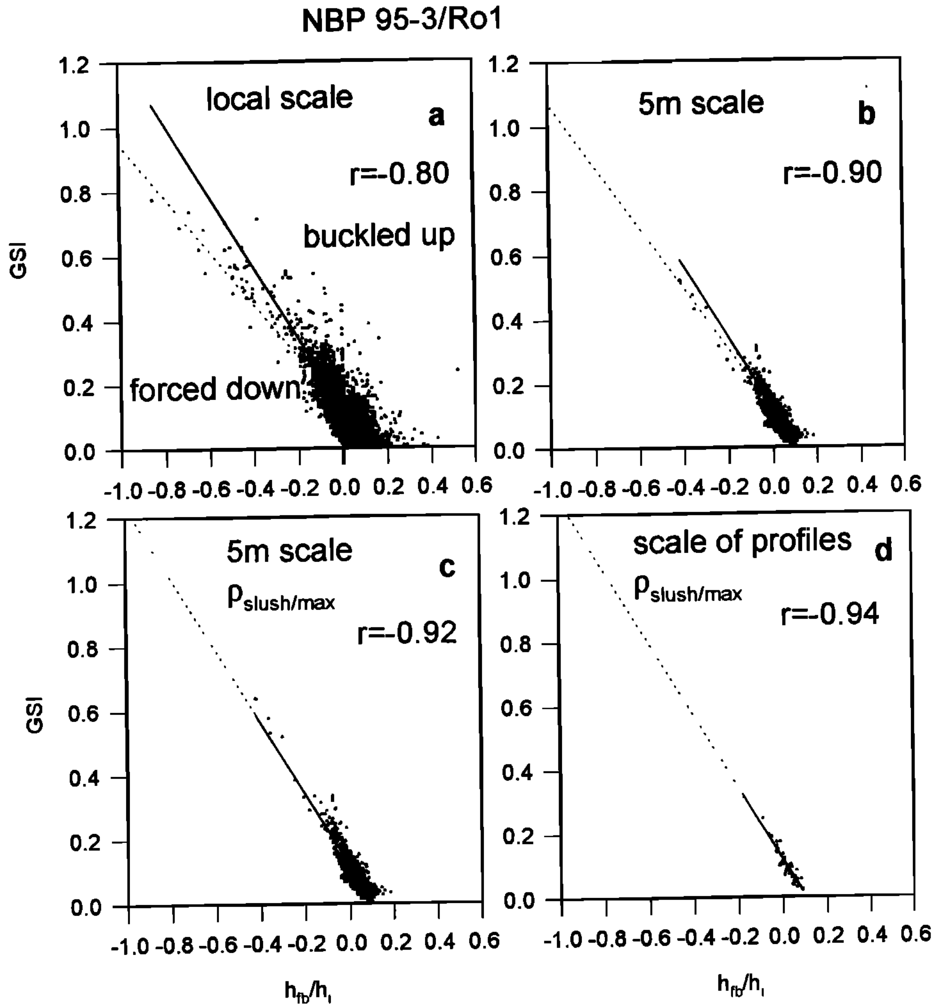

Figure 12. Generalized density-weighted snow/ice thickness ratio (GSI) versus freeboard/ice thickness for all data of the early winter Ross Sea cruise. (a) all data on a local scale, obtained by applying the mean snow density (0.34 g cm-3) and a slush density of 0.70 g cm-3 (highest measured value). (b) Result of a 5 m average. (c) The 5 m average, obtained by applying a maximum slush density of 0.96 g cm-3 (calculated). (d) Result of further averaging to the level of profiles. Lines of regression (dotted lines) can be compared to the isostatic line (solid lines).

In Table 3 the correlation coefficients between GSI and the freeboard to ice thickness values are listed for each cruise for the local scale as well as for the scale of the complete profile. It was found that correlations, estimated with the GSI, provide generally higher correlations as compared to the case where the simpler snow/ice thickness ratio was used.

In conclusion, it can be stated that defining a GSI that includes slush density leads to an improved description of isostatic balance for the sea ice cover. Even on a local level measured points were generally found to be close to isostatic balance. With increasing spatial averaging, a decreasing scatter of the data was observed, indicating that imbalance is a function of scale. Single points that deviate from the line of isostatic balance can be caused by either measuring inaccuracies (mainly in the densities) or by stress-induced local depression or rise of the ice floe.

5.2. Influence of Snow and Slush Density on Isostatic Balance or Imbalance

The analysis of section 5.1 raises the question of how much the choice of the two free density parameters ρ_s and ρ_{sl} can influence the correlations and the agreement between the regression line and the isostatic line.

The use of a mean bulk snow density for each cruise (shown in Figure 12 for NBP 95-3) was superior to using the one or two snow pits available per floe to define separate snow densities for individual floes. This suggests that snow pits on individual floes usually do not provide representative snow densities for these floes. Since the choice of a constant snow density for all floes (zero variance) gives higher correlations, it can also be concluded that the variance of the measured densities between floes exaggerates the variance of the true mean densities per floe. A possibility for improving on the derived mean densities per cruise would be to measure a finely sampled snow density profile parallel to the drill profile for each floe.

More unknowns are involved in the proper choice of the slush density, for which there is no accurate measurement procedure known. Since water is invariably lost during the measurement procedure, it is assumed that even the highest measured values (about 0.70 g cm^{-3}) represent only a lower limit of real slush densities.

Table 3. Correlations Between GSI and Freeboard/Ice Thickness Ratio h_{fb}/h_{ice} for Mean Snow Densities and Different Slush Densities on Two Different Spatial Levels

		Corr.coeff. (GSI to h_{fb}/h_{ice})		
		local scale		scale of profiles
Cruise	$\langle\rho_{snow}\rangle$	ρ_{slush}=0.7	$\rho_{slush/max}$ [a]	ρ_{slush}=0.7
NBP 93	0.36 [b]	-0.43	-0.48	-0.85
NBP 94	0.36	-0.76	-0.81	-0.86
NBP 95-3/Ro1 [c]	0.35	-0.80	-0.83	-0.93
NBP 95-5/Ro2 [d]	0.40	-0.53	-0.58	-0.75
NBP 95-5/Am [e]	0.37	-0.69	-0.72	-0.87

The quantity h_{fb}/h_{ice} was introduced by *Sturm et al.* [1998].

[a] value for maximum slush density according to equation (7).

[b] Value is assumed, since no mean bulk density was calculated for this cruise

[c] Data from early winter Ross Sea (May/June 1995)

[d] Data from late winter Ross Sea (August 1995)

[e] Data from late winter Amundsen and Bellingshausen Seas (August/September 1995)

In the following an upper bound for the slush density is determined from a theoretical standpoint. If snow is viewed as ice particles surrounded by interstitial pockets of air where the density of the latter can be neglected against those of ice and water, one finds ρ_s/ρ_i for the volume fraction occupied by ice particles and $(1-\rho_s/\rho_i)$ for the volume fraction of air. If all air pockets of this "snow sponge" are filled with water one obtains the maximum possible slush density

$$\rho_{sl/\max} = \rho_w - \left(\frac{\rho_w}{\rho_i} - 1\right)\rho_s . \qquad (7)$$

If ρ_w and ρ_i are taken as constants, the value of maximum slush density depends only on the snow density.

Real slush can be assumed to have a density that is smaller than or equal to this maximum density and will depend on the detailed process of slush formation. During the process of flooding, not all air pockets necessarily fill with water and parts of the upper snow pack may fall into the flooded layer, leading to an increase in the ice volume to water volume ratio. Both effects decrease the slush density with respect to (7). For NBP 95-3, with a mean bulk snow density of 0.35 g cm^{-3} [*Sturm et al.*, 1998], (7) gives a maximum slush density of 0.96 g cm^{-3}. Using this value instead of 0.70 g cm^{-3} in Figure 12b on the 5 m scale leads to Figure 12c. One sees that the correlation between the GSI and h_{fb}/h_i has increased and that the agreement between the regression line and the isostatic line has clearly improved. Figure 12d shows that the same situation on larger averaging scales (scale of profiles) can further reduce the variance of the data around the line of regression. Also, for the data sets of the other cruises, it was generally found that the fit of (6) to the data was much improved by using slush densities close to the maximum value.

5.3. Investigations of Single Profiles

Examination of data points measured on single profiles further clarifies how the values for slush and snow densities influence the fit of the data to the isostatic line. Only profiles that cover a sufficient freeboard range are suitable for such an examination.

Figure 13 shows an example of such a profile from the early winter Ross Sea (Figure 13a). Figure 13b shows the GSI versus freeboard/ice thickness ratio for all data (without spatial averaging) using the mean bulk snow density of the particular cruise and 0.70 g cm^{-3} for the slush density. Figure 13c shows that the choice of the maximum slush density substantially improved the fit between the line of regression and the isostatic line. It was generally observed that choosing a slush density close to the maximum value most strongly improved the fit by adjusting the slope of the regression line to the isostatic line. Fine adjustment of the snow density (e.g., from 0.35 to 0.37 g cm^{-3}

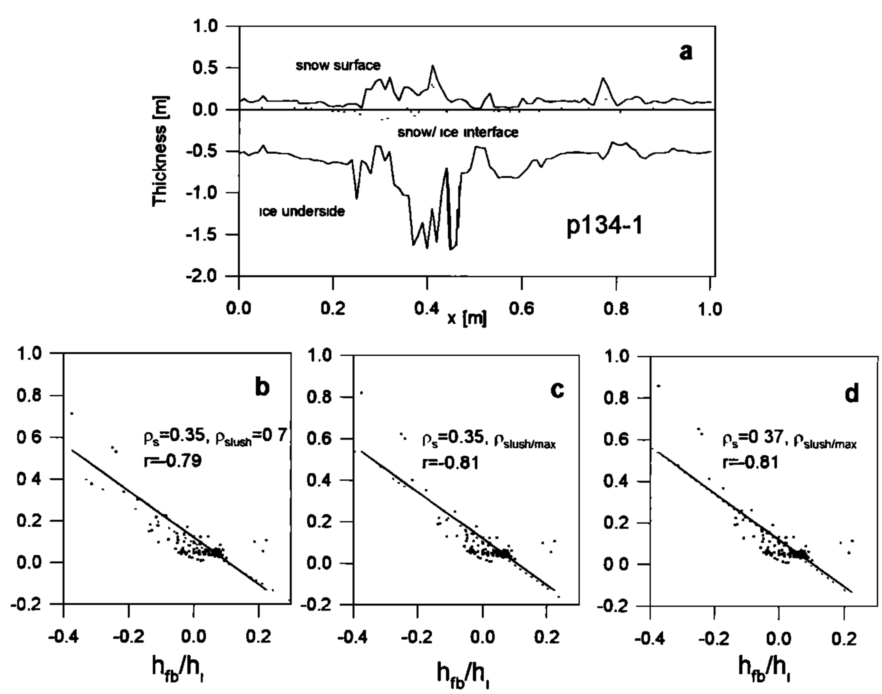

Figure 13. GSI versus freeboard/ice thickness (a) for a single profiles of the early winter Ross Sea. (b)-(d) Lines of regression (dashed lines) approach the isostatic line (solid) by variation of slush and snow density. Data are shown on a local, nonaveraged scale.

from Figure 13d) effects a slight parallel displacement of the regression line. For the particular floe in Figure 13, adjusting the slope of the regression line via the slush density already gives a close match with the isostatic line; adjusting the snow density results in no further significant improvement in this case. However, for a number of other floes, there existed more significant parallel offsets between the two lines, and adjustment of the snow density additionally improved the correlation coefficients for these cases.

6. Isostatic Depression and Uplift of a Floe

Section 5 showed that most floes appear to be isostatically balanced on an averaging scale of a few meters if an appropriate slush density is considered in the isostatic equation. These results suggest that the isostatic uplift and subsidence of a floe may be estimated by idealizing it as being level with a constant snow and ice thickness equal to the mean values of the floe. The following simplified scenarios of snow loading, ice growth, and bottom melting can be applied to this idealized floe (section 6.1). As a further consequence, they can be applied to estimating snow ice growth (section 6.2).

6.1. Snowload, Bottom Melting and Ice Growth

First, subsidence due to increasing snow load will be considered. This process becomes crucial when the upper surface of the floe sinks below the waterline. The assumed level floe is now totally below water, and the snow layer will automatically start to be flooded. This process adds further weight to the snow and ice column, leading to more depression and more flooding. The incremental subsidence of the floe therefore seems to be a never ending process.

In the following it is assumed that below the waterline all the snow is flooded and that all its air pores actually become water logged. If it is further assumed that the snow density at the ice interface is equal to the snow layer on top ($\rho_{sb}=\rho_{st}=\rho_s$), a new snow fall Δx_s will depress the floe by $\Delta x_s\rho_s/\rho_w$ of which, in turn, $(1-\rho_s/\rho_i)$ parts will be filled with water at the bottom of the floe. The infinite summation of the subsidence increments results in the following geometric series:

$$\Delta y_s = \Delta x_s \frac{\rho_s}{\rho_w}\left[1+\left(1-\frac{\rho_s}{\rho_i}\right)+\left(1-\frac{\rho_s}{\rho_i}\right)^2+\ldots\right]=\frac{\rho_i}{\rho_w}\Delta x_s \quad (8)$$

for the value of the depression Δy_s of an isostatically balanced floe with freeboard zero in response to an additional snowload of Δx_s (with ρ_w=1.03 g cm^{-3} and ρ_i = 0.91 g cm^{-3}). It also shows that the floe will find a finite and stable equilibrium, even if the underlying processes are complicated. This new state of the floe is again isostatically balanced.

In a similar fashion, bottom melting creates isostatic subsidence. Melting the ice underneath by Δx_m will make the floe sink by an amount Δy_m which can be derived as

$$\Delta y_m = \frac{1}{\rho_s}\frac{\rho_i(\rho_w-\rho_i)}{\rho_w}\Delta x_m, \quad (9)$$

by solving the isostatic equation (4).

Finally, if one considers how the growth of congelation ice counteracts the above two processes of subsidence (equations (8) and (9)) by isostatically uplifting the floe, one obtains

$$\Delta y_g = -\frac{\rho_i}{\rho_w}\Delta x_g \quad (10)$$

for the uplift in response to an ice growth of Δx_g Here positive and negative y values refer to subsidence and uplift, respectively.

Given these formulas, an order of magnitude comparison between these different processes can be carried out. Comparing (8) to (9) gives roughly 0.8 cm of subsidence per centimeter of snow accumulation and about 0.3-0.5 cm (corresponding to a snow density ranging between 0.2 and 0.4 g cm^{-3}) subsidence per centimeter of ice melt. This finding is close to the results of *Ackley et al.* [1990] who suggested a rough balance between snow ice growth and loss of ice from bottom melting in the eastern Weddell Sea. It should be noted, however, that for bottom melting to occur, ice surface temperatures should not fall below -5°C and oceanic heat fluxes should be at least as high as 20-30 W m^{-2} as shown by *Lange et al.*[1990]. While mean bottom melt rates of 0.4 cm d^{-1} [*Lange et al.*,1990; *Ackley et al.*, 1995] occurred in the eastern Weddell Sea, studies in the western Weddell Sea [*Lytle and Ackley*, 1996] showed actual oceanic heat fluxes between 4 and 12 W m^{-2}, which makes ice melt very unlikely in this region.

If a net snow accumulation rate of 0.01 cm d^{-1} [*Parkinson*, 1982; *Bromwich*, 1990] and the above melt rate of 0.4 cm d^{-1} are assumed, the combined daily subsidence due to snow load and bottom melting ranges between 0.13 and 0.21 cm d^{-1}. Application of an ice growth rate of 0.4 cm d^{-1}, suggested by *Wadhams et al.* [1987] for the eastern Weddell Sea, to (10) gives about 0.35 cm d^{-1} uplift due to ice growth. This shows that in regions where bottom melting occurs, subsidence can be of similar magnitude to uplift, due to ice growth.

6.2. Estimation of snow ice growth

A simple gedankenexperiment can be carried out to determine the snow ice growth between the early and late winter Ross Sea cruises from mean thickness values for snow, ice and freeboard spaced 3 months apart (see Table 1). As a first step, a layer of snow that accounts for the snow ice formation Δx_{si} between the two cruises needs to be added to the difference in measured snow thickness Δx_s. As a second step the layer of snow that did not contribute to flooding and snow ice formation has to be subtracted. The effective snow layer Δx_s^{eff}, which is significant for flooding and snow ice formation thus can be calculated as

$$\Delta x_s^{\text{eff}} = \left[\Delta x_s + \Delta x_{si}\frac{\rho_i}{\rho_w}\right] - \left\{\left[fb_1 + |\Delta y_g(\Delta x_g)|\right]\frac{\rho_i}{\rho_s}\right\}, \quad (11)$$

where fb_1 is the positive mean freeboard of the first Ross Sea cruise and $\Delta y_g(\Delta x_g)$ is the uplift due to congelation ice growth Δx_g according to (10). It can be seen that the first bracketed expression in (11) is the sum of the actual measured difference in snow thickness plus the additional layer of snow that would have been measured if it had not been transformed to snow ice. The second bracketed expression describes the part of the snowfall that did not contribute to flooding and snow ice formation. The difference between both expressions is thus the effective snow layer Δx_s^{eff} that induced flooding and/or snow ice formation. Further, the total measured ice growth Δx_i is given by

$$\Delta x_i = \Delta x_g + \Delta x_{si},$$

the sum of congelation ice growth and snow ice growth. The depression Δy_s due to the effective snow layer Δx_s^{eff} is, according to (8)

$$\Delta y_s\left(\Delta x_s^{\text{eff}}\right) = \Delta x_{si}\frac{\rho_i}{\rho_w} - fb_2,$$

where fb_2 is the mean, negative freeboard value of the second, late winter Ross Sea cruise. Assuming again ($\rho_{sb}=\rho_{si}=\rho_s$), the final equation for determining the snow ice growth Δx_{si} therefore becomes

$$\Delta x_{si} = \frac{\left(\Delta x_s - \frac{\rho_i}{\rho_s} fb_1 - \frac{\rho_i^2}{\rho_s \rho_w} \Delta x_i + \frac{\rho_w}{\rho_i} fb_2\right)}{\left(1 - \frac{\rho_i}{\rho_w} - \frac{\rho_i^2}{\rho_s \rho_w}\right)}. \tag{12}$$

Inserting Δx_s = 11 cm for the mean snow accumulation, Δx_i =12 cm for the mean ice growth between the two Ross Sea cruises, fb_1 = 1.4 cm and fb_2 = -0.3 cm for the corresponding freeboard values (Table 1) and ρ_s = 0.37 g cm^{-3} (Table 3) for the mean snow density gives 9.1 cm of mean snow ice growth compared to 2.9 cm of congelation ice growth in the course of 3 months. It can be concluded that under simplified, isostatically balanced conditions, which exclude any deformation processes, snow ice formation would be the major contribution to the overall ice growth.

7. Conclusions and Discussion

Five snow and ice thickness data sets of south polar Pacific sea ice floes visited in 1993-1995 were intercompared. Level ice thicknesses of the late winter cruises (Table 1) were found similar to values reported by *Lange and Eicken* [1991] for undeformed first-year ice in the northwestern Weddell Sea in 1989 (75 cm). However, the winter values presented here are somewhat higher than those found in East Antarctica in late winter [*Allison and Worby*, 1994]. Even if a detailed comparison is limited by differences in sampling methods, it can be generally concluded that level ice thicknesses for all cruises were similar or slightly higher than in other Antarctic regions.

The Amundsen and Bellingshausen Seas can be characterized as regions of persistent deformation, whereas the pack ice in the atmospherically calmer and more protected Ross Sea embayment is less dominated by ridging and rafting. As a result distribution functions for the ice of the Amundsen and Bellingshausen Seas are more irregularly shaped and show a broader range of ice thicknesses. Together with the snow and ice thickness data, freeboard distributions from the Ross Sea in early and late winter suggest a seasonal increase of snow ice formation.

The potential for snow ice formation was also studied directly: A thorough investigation of the drilling area prior to the actual drilling process revealed how much moisture, wetness and flooding of an undisturbed floe are related to subsequent negative freeboard measurements. There was a good correlation with negative freeboard at places where flooding had occurred and a lesser correlation where the snow was only moist. Moisture, wetness and flooding are well correlated to the ratio of snowload to ice thickness while the relation to the amount of ridging is less conclusive. The maximum possible effect of freeboard disturbance due to ice floe deflection from the weight of the field party was estimated to be 1.6 cm.

Correlations between snow load, ice thickness, and freeboard were examined. Isostatic balance was investigated in detail on various spatial scales by introducing an isostatic balance equation that includes an explicit slush density to account for flooding and ongoing snow ice formation. Using the improved isostatic balance equation, deviations from isostatic equilibrium were shown to occur only locally and to decrease quickly on spatial averaging scales of a few meters, even for heavily ridged areas. Exact fits of the data to isostatic equilibrium showed a consistent dependence on slush and snow densities. The choice of the maximum possible slush density most always improved the fit substantially, whereas the adjustment of the snow density in some cases effected a further fine scale improvement. This method of adjusting the two density parameters can therefore be proposed for cases where measured densities in snow pits are considered not to be representative for the respective floe.

With the help of a simple isostatic model the effect of increasing snow load, bottom melting, and ice growth on the depression and uplift of a floe could be calculated. This also allowed to make an estimate of how much snow ice growth contributes to the total ice growth.

Acknowledgments. Data acquisition was made possible by NSF grants OPP-9117721 and OPP-9316767 (principal investigator Martin Jeffries). For their worthwhile scientific comments I want to thank Will Harrison, Paul Layer, Lewis Shapiro, Matthew Sturm, Willy Weeks and Gunter Weller. I also want to address my special thanks to the following people who contributed to the acquisition of snow and ice thickness data during four cruises: André Belem, Dave Crane, Liz Chilton, Kent Chen, Mark Cochrane, Jim Cooper, Stephanie Cushing, Chris Fritsen, Joanne Groves, Gwyneth Hufford, Barbara Hurst-Cushing, Ricardo Jaña, Barney Kane, Lyle Lawbaugh, Erika Lawson, Matt Lawson, Ted Maksym, Rod McCabe, Rob Massom, Shawn McCullars, Kim Morris, Doyle Nicodemus, Russ Nilson, Janet Nonelly, Greg Packard, Marjorie Porter, Tim Quakenbush, Bernhard Rabus, Blaine Reynolds, Joe Sapiano, Buzz Scott, Chuah Teong Sek, Jennifer Simmons, Randy Sliester, Jane Stevens, Dave Stokes, Mark Talkovich, Willy Weeks, Tony Worby, and Bill Young. For logistics, Captain Joe Borkowski and his crew on board of the *Nathaniel B. Palmer* should be thanked. I wish to thank J. A. Richter-Menge and two anonymous reviewers whose comments helped to improve an earlier version of the manuscript.

References

Ackley, S. F., A review of sea-ice weather relationships in the Southern Hemisphere, in *Sea Level, Ice, Climate*, IAHS Publ., *131*, 127-159, 1981.

Ackley, S. F. and T. E. Keliher, Antarctic sea ice dynamics and its possible climatic effects, *AIDJEX Bull.*, *33*, 53-56, 1976.

Ackley, S. F. and C. W. Sullivan, Physical controls on the development and characteristics of Antarctic sea ice biological communities - a review and synthesis, *Deep Sea Res. Part I*, *41*, 1583-1604, 1994.

Ackley, S. F., M. A. Lange and P. Wadhams, Snow cover effects on Antarctic sea ice thickness, in Sea Ice Properties and Processes, *CRREL Monograph 90-1* edited by S.F. Ackley and W.F. Weeks, pp. 16-21, Cold Reg. Res. and Eng. La.b., Hanover, N.H., 1990.

Allison, I., The East Antarctic sea ice zone: ice characteristics and drift, *GeoJournal*, *18 (1)*, 103-115, 1989.

Allison, I. and A. P. Worby, Seasonal changes of sea-ice characteristics off East Antarctica, *Ann. Glaciol.*, *20*, 195-201, 1994.

Allison, I., R. E. Brandt and S. G. Warren, East Antarctic sea ice: albedo, thickness distribution and snow cover, *J. Geophys. Res.*, *98*(C7), 12,417-12,429, 1993.

Bromwich, D. H., Estimates of Antarctic precipitation, *Nature*, *343*, 627-628, 1990.

Budd, W. F., Antarctic sea ice variations from satellite sensing in relation to climate, *J. Glaciol.*, *15*, 417-427, 1975.

Carleton, A. M., Monthly variability of satellite-derived cyclonic activity for the SouthernHemisphere winter, *J. Climatol.*, *1*, 21-38, 1981.

Cavalieri, D. J. and C. L. Parkinson, Large-scale variations in observed Antarctic sea ice extent and associated atmospheric circulation, *Mon. Weather Rev.*, *109*, 2323-2336, 1981.

Comiso, J. C., P. Wadhams, W. B. Krabill, R. N. Swift, J. P. Crawford and W. B. Tucker III, Top/bottom multisensor remote sensing of Arctic sea ice, *J. Geophys. Res.*, *96*(C2), 2693-2709, 1991.

Dierking, W., Laser profiling of the ice surface topography during the Winter Weddell Gyre Study 1992, *J.Geophys.Res.*,*100*(C3), 4807-4820, 1995.

Drinkwater, M. R., D. G. Long and D. S. Early, Enhanced resolution scatterometer imaging of Southern Ocean sea ice, *ESA Bull.*, *17*, 307-322, 1993.

Eicken, H., M. A. Lange, H. W. Hubberten, and P. Wadhams, Characteristics and distribution patterns of snow and meteoric ice in the Weddell Sea and their contribution to the mass balance of sea ice, *Ann. Geophys.*, *12*, 80-93, 1994.

Eicken, H., H. Fischer, and P. Lemke, Effects of the snow cover on Antarctic sea ice and potential modulation of its response to climatic change, *Ann. Glaciol.*, *21*, 369-376, 1995a.

Eicken, H., M. Lensu, M. Leppaeranta, W. B. Tucker, A. J. Gow, and O. Salmela, Thickness, structure, and properties of level summer multiyear ice in the Eurasian sector of the Arctic ocean, *J. Geophys. Res.*, *100*(C11), 22,697-22,710, 1995b.

Fletcher, J. O., Ice extent on the southern ocean and its relation to world climate, *Memo.* RM-5793-NSF, Rand Corp., Santa Monica, California, 1969.

Fritsen, C. H., V. I. Lytle, S. F. Ackley and C. W. Sullivan, Autumn bloom of Antarctic pack-ice algae, *Science*, *266*, 782-784, 1994.

Gordon, A. L., Seasonality of Southern Ocean sea ice, *J.Geophys.Res.*, *86*(C5), 4193- 4197,1981.

Gordon, A. L. and H. W. Taylor, Seasonal change of Antarctic sea ice cover, *Science*, *87*, 346-347, 1975.

Hibler, W. D., III, and S. F. Ackley, Numerical simulations of the Weddell Sea pack ice, *J. Geophys. Res.*, *88*(C5), 2873-2888, 1983.

Hosseinsmostafa, A. R., V. I. Lytle, K. C.Jezek, S. P. Gogineni, S. F. Ackley, and R. K.Moore, Comparison of radar backscatter from Antarctic and Arctic sea ice, *J. Electromagn. Waves Appl.*, *9*(3), 421-438, 1995.

Jacobs, S. S. and J. C. Comiso, Sea ice and oceanic processes on the Ross Sea continental shelf, *J.Geophys.Res.*, *94*(C12), 18,195-18,261, 1989.

Jeffries, M. O. and U. Adolphs, Early winter ice and snow thickness distribution, ice structure and development of the western Ross Sea pack ice between the ice edge and the Ross ice shelf, *Antarc.Sci.*, *9*(2), 188-200, 1997.

Jeffries, M. O., K. Morris, A. P. Worby and W. F. Weeks, Late winter sea ice properties and growth processes in the Bellingshausen and Amundsen Seas, *Antarct. J. U.S.*, 29, 11-13, 1994.

Lange, M. A., P. Schlosser, S. F. Ackley, P. Wadhams, and G. S. Dieckmann, ^{18}O concentrations in sea ice of the Weddell Sea, Antarctica, *J. Glaciol.*, *36*, 315-23, 1990.

Lange, M. A., and H. Eicken, The sea ice thickness distribution in the Northwestern Weddell Sea, *J. Geophys.Res.*, *96*(C3), 4821-4837, 1991.

Ledley, T. S., Snow on sea ice: Competing effects in shaping climate, *J. Geophys. Res.*, *96*(D9),17,195-17,208, 1991.

Ledley, T. S., Sea ice: A factor in influencing climate on short and long time scales, in *Ice in the Climate System*, edited by W. Peltier, pp 532-556, Springer-Verlag, New York, 1994.

Lytle, V. I., and S. F. Ackley, Heat flux through sea ice in the western Weddell Sea: Convectice and conductive transfer processes, *J.Geophys.Res.*, *101*(C4), 8853-8868, 1996.

Martinson, D., Ocean heat and sea ice thickness in the Southern Ocean, in *Ice in the Climate System*, edited by W. Peltier, pp. 597-610, Springer-Verlag, New York, 1994.

Massom, R. A., M. R. Drinkwater, and C. Haas, Winter snowcover sea ice in the Weddell Sea, *J.Geophys.Res.*, *102*(C1), 1101-1117, 1997.

Maykut, G. A., Energy exchange over young sea ice in the Central Arctic, *J.Geophys.Res.*, *83*, 3646-3658, 1978.

Parkinson, C., Sensitivity studies on a model of the Weddell ice pack, *Antarct. J. U.S.*, *17*, 94-95, 1982.

Parmerter, R. R., A mechanical model of rafting, *AIDJEX Bull.*, *23*, 97-115, 1974.

Perovich, D. K. and J. A. Richter-Menge, Surface characteristics of lead ice, *J.Geophys.Res.*, *99*(C8), 16,341-16,350, 1994.

Streten, N. A., and D. J. Pike, Characteristics of the broadscale Antarctic sea ice extent and the associated atmospheric circulation 1972-1977, *Arch. Meteo. Geophys. Bioklimatol.*, Ser. A, *A29*, 279-299, 1980.

Sturm, M., K. Morris, and R. Massom, The winter snow cover of the West Antarctic pack ice: Its spatial and temporal variability, in *Antarctic Sea Ice, Antarct. Res. Ser.*, vol. 74, edited by M. O. Jeffries, pp. 1-18, AGU, Washington, D.C., 1998.

Sturman, A. P., and M. R. Anderson, On the sea-ice regime of the Ross Sea, Antarctica, *J. Glaciology, 32*, 54-59, 1986.

Turcotte, D. L., and G. Schubert, *Geodynamics*, 450 pp., Wiley, New York, 1982.

Wadhams, P. and R. J. Horne, An analysis of ice profiles obtained by submarine sonar in the Beaufort Sea, *J.Glaciol.*, *25*(93), 1980.

Wadhams, P., M. A. Lange, and S. F. Ackley, The ice thickness distribution across the Atlantic sector of the Antarctic Ocean in midwinter, *J.Geophys.Res.*, *92*(C13), 14,535 -14,552, 1987.

Wadhams, P., W. B. Tucker III, W. B. Krabill, R. N. Swift, J. C. Comiso and N. R. Davis, Relationship between sea ice freeboard and draft in the Arctic basin, and implications for ice thickness monitoring, *J.Geophys.Res.*, *97*(C12), 20,325-20,334, 1992.

Weeks, W. F., W. B. Tucker III, M. Frank and S. Fungcharoen, Characterization of surface roughness and floe geometry of sea ice over the continental shelves of the Beaufort and Chukchi Seas, in *Sea Ice Processes and Models*, edited by R. S. Pritchard, pp. 301-312, Univ. of Wash. Press, Seattle, 1980.

Worby, A. P., W. F. Weeks, M. O. Jeffries, K. Morris and R. Jaña, Late winter sea ice and snow thickness distribution in the Bellingshausen and Amundsen Seas, *Antarct. J. U.S.*, *29*, 13-15, 1994.

Worby, A. P., M. O. Jeffries, W. F. Weeks, K. Morris, and R. Jaña, The thickness distribution of sea ice and snow cover during late winter in the Bellingshausen and Amundsen Seas, Antarctica, J. Geophys. Res., 101(C12), 28,441-28,455, 1996.

U. Adolphs, Weissenburger Platz 6b, 81667 Munich, Germany. (e-mail:uadolphs@t-online.de)

(Received August 25, 1997; revised June 5, 1998; accepted July 7, 1998.)